AFM and X-ray Studies of Crystal and Ionic Domain Morphology in Poly(ethylene-*co*-methacrylic acid) Ionomers

Bryan B. Sauer* and R. Scott McLean

DuPont Central Research and Development, Experimental Station, Wilmington, Delaware 19880-0356

Received June 27, 2000

ABSTRACT: New AFM methods were applied to resolve the morphology of the ionic domains in poly(ethylene-*co*-methacrylic acid) copolymers. Using standard tapping AFM techniques with a precision in the lateral dimensions on the order of a nanometer, the crystalline lamellar structure and overall morphology consisting of stacks of ethylene-rich lamellae separated by sometimes broad noncrystalline regions were characterized. By operating the AFM under special low oscillation amplitude conditions where tip−ionic cluster interactions could be induced to dominate the phase signal, it was shown that this method could be used to uniquely resolve ionic-rich regions and individual ionic domains. The individual domains were found to be on the order of 2 nm in diameter. Small-angle X-ray scattering (SAXS) characterization was used to confirm some aspects of the morphology and to contrast the different levels of resolution of the two techniques for both lamellar crystals and ionic domains. By sequential images taken under different tapping AFM conditions, the "softer" amorphous regions were found to be the richest in ionic domains. Lamellar morphology and perfection were found to be controlled by mobility in the melt which depends on acid level, neutralization level, and counterion type in the different ionomers studied. The crystalline domains in the metal neutralized ionomers were compared to the unneutralized "acid" form of the ionomer. Data for the acid form verified that no ionic domains exist in this material.

Introduction

Ionomers such as poly(ethylene-*ran*-methacrylic acid) neutralized with Zn and other metal ions are examples of the Surlyn family of copolymers. Ionic clustering in many polymers including these ethylene-based ionomers,[1−6] perfluorinated sulfonic acid,[3,6−11] and other ionomers[2−6,12] based on block copolymers has been reviewed. Theoretical models for ionic clustering describe the energetics and chain conformation effects in limiting cluster sizes.[3−9,12] Some theories have been criticized because they do not consider the constraints imposed by the crystallites.[3] Complete theories are apparently unavailable because of the many complexities including energetics of ion interactions, steric chain effects, interfacial tension and interface interactions, and possibly chain mobility constraints due to crystallinity. The importance of the latter must be qualified because even in the melt there are ionic domains comparable in size which contribute to small-angle X-ray scattering,[2,13] strongly suggesting that steric chain constraints[12] are dominant in limiting ionic domain size.

The nature of steric effects involving the chain structure includes the covalent attachment of hydrocarbon chains to the ionic groups and forms the basis of the model of Yarusso and Cooper[2,14] where the distance between ionic domains depends on both the diameter of the ionic domain and the thickness of the attached hydrocarbon chains at the "surfaces" of the domains. The morphology studies based mostly on small-angle X-ray scattering (SAXS) show that this model of interionic domain scattering provides an excellent description of many ionomer systems, and the results show that other models may be less applicable.[2] Effects of dispersity of domain spacings are probably important but have not been considered.

Although the influence of polymer structures on the domain spacings is relatively well established, studies of domain size are very controversial. The results on different polymers show interesting structure/property relationships of ionic domain size,[2] but the absolute domain sizes are qualitative because of possible model-dependent contributions to the analysis. The detailed relationship of domain sizes to the semiblocky structure of the polymer chain with ionic species separated by hydrocarbon blocks of different length in different Surlyn compositions is not available. In one early model,[12] chain structure and the energetics of chain stretching resulting from steric effects due to the copolymer chain structure were considered in addition to the ionic interactions. Related to this is the steric constraints which evolve due to the accumulation of hydrocarbon chains around the ionic domains (or other "hard" domains) at a given volume fraction of ionic species, and these could provide kinetic limitations to domain formation.

SAXS,[1,2,6,7,10,11,13] neutron scattering,[15] transmission electron spectroscopy (TEM),[6] and dynamic mechanical data[5,6] all can be qualitatively correlated with various model predictions.[5] From the start,[2,16−18] interpretation of the SAXS peak associated with the ionic domains has been controversial in poly(ethylene-*ran*-methacrylic acid) ionomers. The "higher angle" SAXS peak maximum was attributed to either interparticle or intraparticle scattering, and several diverse ionic domain morphologies were postulated including sphere,[2] lamellae,[17] and core/shell.[18] Recent experiments using extended X-ray absorption fine structure spectroscopy also provide detailed information about the coordination number and chemistry of the ionic species[19,20] and provide some evidence that is consistent with nonspherical ionic domains.[20] Recent scanning (STEM) data have provided new direct evidence of a spherical shape,[21,22] the STEM[21,22] studies characterized domain diameters of approximately 2−3 nm for Zn-neutralized Surlyn,[21,22] and the domains are found to have a relatively low level of dispersity in sizes with sizes only slightly dependent

10.1021/ma001110t CCC: $19.00
Published on Web 09/16/2000

on neutralization level. The STEM results[22] provide valuable model-independent characterization of domain size and shape which suggests that many available theoretical models referenced above are not accurate and should be refined. They strongly suggest that the earlier estimates of domain diameters on the order of 1 nm for Surlyn[2,12] are far too small. Additional SAXS studies including "resonant" SAXS studies,[23] which use wavelength to change the contrast due to the presence of metal ions, have provided additional details of ionic domain morphology.

Because the electron microscopy section thickness is not exactly controlled and is large relative to the ionic domain size, the position in space of ionic domains relative to the ethylene crystal aggregates (i.e., stacks of lamellae) is difficult to discern. In addition, the overall phase structure and organization including the polyethylene lamellae are not easily resolvable by electron microscopy because of the high degree of imperfection of the ethylene crystals. The low degree of order also leads to difficulties in modeling of SAXS data and to difficulties in characterization by wide-angle X-ray diffraction in ionomers and other ethylene copolymers where WAXD gives a total percent crystallinity much lower than that derived from DSC and other techniques because of the poor crystal perfection.[24,25]

Recent work has verified that tapping AFM has resolution similar to that of TEM for some polymer morphological features such as crystal lamellae near the surface,[26−31] with the additional advantage of AFM that thin sections are not needed. It has been demonstrated that AFM can resolve certain polymer microstructural features at the nanometer scale, with the limitation that the particular orientation and depth of domains under the surface can modify aspects of the actual resolution of such features.[27,28,32] However, the application of AFM in the ionomer field has mainly addressed surface textural features,[33−35] and only recently have new AFM methods been developed and applied to the examination of ionic clusters.[36] We will discuss data which show that a combination of AFM techniques can provide additional morphological information not readily available from any other real-space technique because of the ability of AFM to characterize the ethylene lamellae in addition to using novel imaging methods[36] to determine the relative morphological position of the ionic species and domains. The real space organization and network of ionic and nonpolar aggregates is relevant to transport,[3,7−9] surface, adhesion, and mechanical properties.[4] We will also contrast the results with new SAXS data on some of the systems in an attempt to obtain a more detailed picture of ionic domain morphology.

Experimental Section

Materials and Preparation. The Surlyn samples are from DuPont and are based on poly(ethylene-*co*-methacrylic acid) polymers. These are metal neutralized with the degrees of neutralization and acid comonomer levels listed in Table 1 and a sample designation implemented by indicating the metal neutralization species followed by the degree of neutralization, e.g., Zn58 for 58% neutralization. The ethylene blocks form crystallites which are characterized by broad melting DSC regions with peak melting points around 90−110 °C depending on the composition,[23] which can be compared with a melting point for linear polyethylene of about 133 °C.

Surfaces with low levels of long-range roughness can improve resolution of nanocrystal structures in tapping AFM studies.[28] Obtaining smooth surfaces from the melt for polymers that crystallize can be difficult because crystallization in some polymers roughens the surface. Because of this, we developed methods to fabricate very smooth surfaces for the ethylene-based ionomers, although problems with roughness are less severe with copolymers due to lower degrees of crystallinity. Thermal melt or "melt-pressed" surfaces were obtained by pressing a silane grafted silicon disk onto the Surlyn melt at 180 °C and cooling to room temperature. In some cases the samples were annealed at elevated temperatures. The levels of crystallinity present near the surface are probably difficult to control, and there was no attempt at determining quantitative reproducibility of levels of crystallinity.

Table 1. Summary of AFM Crystal Dimensions and Other Lamellar Properties[a]

	L_{SAXS} (nm)	$l_{c,AFM}$ (nm)[b]	L_{AFM} (nm)[c]	length (nm)[d]
Na54 (Na,10% acid, 54% neut)	8.8	5	6−8	30
Zn18 (Zn, 8.7% acid, 18% neut)	10	5−7	11	50−100
Zn58 (Zn, 15% acid, 58% neut)		7−8	12	40−50
Na59 (Na, 15% acid, 59% neut)	8	5−6	8	15
Nucrel (15% acid, 0% neut)		8−10	15−20	100−200

[a] Neutralizing metal species, weight percent acid in the base polymer, and percent acid groups neutralized are given. [b] $l_{c,AFM}$ = crystal thickness perpendicular to the plane of the lamellae. [c] L = spacing or long period between crystals. [d] Average length of crystals in the long direction.

To coat the silicon wafer, a self-adsorbed monolayer of octadecyltrichlorosilane was deposited from standard hexadecane mixed solvents.[37] The silicon disk was removed from the Surlyn surface after cooling from the melt, leaving a surface almost as smooth as the silicon wafer. This type of silicon surface treatment prevents reaction of materials such as molten nylon and Surlyn with the Si−OH groups on the inorganic oxide surface of the bare silicon, thus minimizing adhesion and acting as a permanent mold release. For the most part the silane remains on the silicon wafer. Evidence for this includes the fact that a single treated disk can be used to prepare several dozen samples from the melt. In one example discussed at the end of this paper, we do note the interesting consequences of degradation of this silane layer. This sample preparation method can be contrasted with a common method typically used in the literature which is to rub polymer on a substrate, sometimes at elevated temperatures. This leaves thin layers with interesting morphologies,[27] but the relationship to morphologies in macroscopically thick samples is sometimes tenuous.

Methods. SAXS data were collected using a compact Kratky camera using Cu Kα (λ = 1.54 Å) radiation. The data were processed after background subtraction and desmearing.

A TA Instruments (Newcastle, DE) 2920 DSC was used for the thermal characterization.

Tapping mode AFM was used to obtain height and phase imaging data simultaneously on a Nanoscope IIIa from Digital Instruments, Santa Barbara, CA. Microfabricated cantilevers or silicon probes (Nanoprobes, Digital Instruments) with 125 μm long cantilevers were used at their fundamental resonance frequencies which typically varied from 270 to 350 kHz depending on the cantilever. Very small tip radii (5−10 nm) and stiff cantilevers are necessary for the ∼1 nm lateral resolution needed for these studies. The images presented here are not filtered.

In tapping mode where the tip makes intermittent contact with the surface. The tapping forces are roughly adjusted by the ratio ($R = A_{eng}/A_{free}$) of the engaged (A_{eng}) or set point amplitude to the free air amplitude (A_{free}),[27] keeping the frequency relative to the resonance peak controlled on the low-frequency side[32,38] to avoid artifacts. This ratio of amplitudes which are used in feedback control was adjusted to R = 0.4−0.7 for "moderate force" imaging (or normal tapping),[27,32] with a free air amplitude of ∼50 ± 10 nm. It is known that these phase lag data are sensitive to local stiffness differences of species or domains in the top several nanometers from the outermost surface.[27,28,32,38]

By operating at lower amplitudes of oscillation of about 8 ± 3 nm,[36] phase lag data that are insensitive to stiffness with certain systems can be obtained with appropriate experimental control. The ratio of tip oscillation amplitudes (R) for low oscillation amplitude imaging conditions were adjusted to the same ratios as for our normal tapping conditions. Recent work has shown that this lower energy applied to the cantilever allows one to directly image the ionic clusters at or near the surface.[36] By lowering the oscillation amplitude of the cantilever, it is possible that attractive tip interactions with the polar ionic domains can dominate the AFM phase signal, giving rise to relatively high contrast in the absolute magnitude of the phase shift. As discussed below, the unneutralized acid form of Surlyn and other controls were used to prove that polar domains cannot be detected unless they are present as aggregates containing ionized species in this low oscillation amplitude mode.

A third method utilizes a very light tapping force[39] and was used to look for polar domains or contrast based on hydrophobicity differences at the outer few angstroms of the surface, i.e., a closer to true surface-specific imaging technique. This mode is implemented by keeping the free air oscillation amplitude the same as in normal tapping (i.e., 50 nm), but R is increased substantially to about 0.9 ± 0.05 reducing the tip to surface interaction forces substantially.[39] Again, this method is useful for determining surface composition of the outermost fraction of a nanometer. Ionic species are not required for contrast in this mode, and the contrast is dominated by hydrophobicity differences and not stiffness differences.[39] No contrast was obtained in images for any of the Surlyn surfaces imaged using this AFM technique. Water contact angles on fresh Surlyn surfaces demonstrate a surface composition similar to pure polyethylene, so presumably the very light tapping method is also detecting a hydrocarbon layer coating the entire outermost fraction of a nanometer of the surface.

Details of the AFM phase imaging methods were presented recently,[36] and a brief summary is as follows:

1. Normal tapping under moderate forces uses stiffness contrast to resolve domains from the top surface down to about 5−10 nm.

2. Low oscillation amplitude tapping is a new method which resolves ionic domains down to ∼2−5 nm below the surface. Ionic species or domains are necessary for contrast in this method of imaging.

3. Very light tapping[39] is sensitive to hydrophobicity differences in the outermost fraction of a nanometer of the surface. Ionic species are *not* necessary for contrast. Certain rough surfaces cannot be studied in this mode.[39]

Results

Several small-angle X-ray scattering studies have characterized details of morphology including the ionic clusters and the "lamellar" crystals of the ethylene-rich segments in Surlyn. Data for Surlyn Zn18, Na54, and Na59 are shown in Figure 1 (see Table 1 for compositions). The maxima at low angles are the Bragg peaks from the stacking of the ethylene lamellae. Lorentz corrections[40,41] are needed for the low angle peak because the lamellae are anisotropic in two dimensions. The correction is simply performed by multiplying the y-axis intensity by the momentum transfer squared, q^2 ($q = 2\pi/(\lambda) \sin 2\theta$), with 2θ the scattering angle. Long periods [$L = 1.54$ Å$/(2\theta_{max})$] obtained are only slightly different for corrected and uncorrected data. Values from corrected data are 10, 8.8, and 8.0 nm for Zn18, Na54, and Na59, respectively. These compare well with those determined directly by AFM for lamellae oriented approximately perpendicular to the surface (Table 1). The broad peaks at $2\theta_{max} \sim 4°$ are due to the interionic domain spacings, and for such isotropic (spherical[21,22]) objects no Lorentz correction should be applied.[40] Figure 1 shows the small shifts in the peaks for such correction

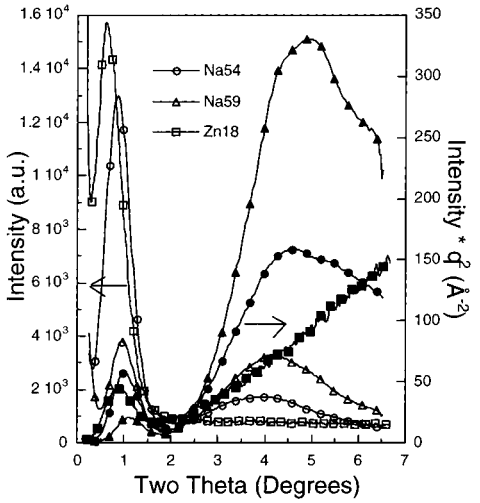

Figure 1. Small-angle X-ray data for samples prepared by cooling from 190 to 25 °C. Sample compositions based on numbers given in the legend can be found in Table 1.

procedures, except in the case of Zn18 where no higher angle peak was detected due to the low level of ionic species. Even though no peak is detected in SAXS, the presence of ionic domains is verified by STEM[22] and also AFM described below, helping to confirm that the "ionic peak" in SAXS is from interparticle scattering and not intraparticle. Since the uncorrected data should be used, these convert to interparticle distances of about $L_{IP} = 2.1$ nm [center-to-center distance $= L_{IP} = 1.54$ Å$/(2\theta_{max})$], and the domain diameters from SAXS have been estimated to be about $d = 1.7$ nm for related Surlyn systems[42] or $d = \sim 2$ nm from TEM.[21,22] The relatively large diameter which is comparable to L suggests that ionic domains are quite close together on average; i.e., the diameters are large enough that there is reduced space between ionic domains for these two systems with relatively high acid and neutralization levels. The cause of this is the exclusion from the crystalline ethylene-rich lamellae and possibly a partial exclusion of ionic species and domains from the interior of lamellar "stack" regions, causing a concentration of ionic domains outside of the lamellar region as confirmed by AFM data below.

Simultaneously obtained AFM height and phase data for Surlyn Zn18 were obtained under normal tapping conditions (Figure 2A,B) and low oscillation amplitude tapping (Figure 2C,D). The total scan boxes for (A)−(D) are 500 nm × 500 nm. In the plots white is high in topography and high in phase, and high phase indicates high stiffness regions in normal tapping (Figure 2B). Generally, in normal tapping with carefully controlled frequencies relative to the cantilever resonance peak, the hard domains are high regions because of higher deformability of the soft phase by the tip,[28] and the stiff regions are also high in phase.[27,28] The ionic domains are not sensed or imaged in these height or phase data obtained under normal tapping conditions (Figure 2A,B). They should reside outside of the hard crystal "lamellae" in softer (darker) amorphous phase regions. The ethylene lamellae show organization into parallel orientations to differing degrees and are relatively well perfected because of the low degree of neutralization of this Surlyn. As with most polymers of this type,[28,38] the outermost layer of the surface is covered with about 1 nm of amorphous material. Amorphous polyethylene segments are the low-energy component and probably dominate the outermost surface. We must image through

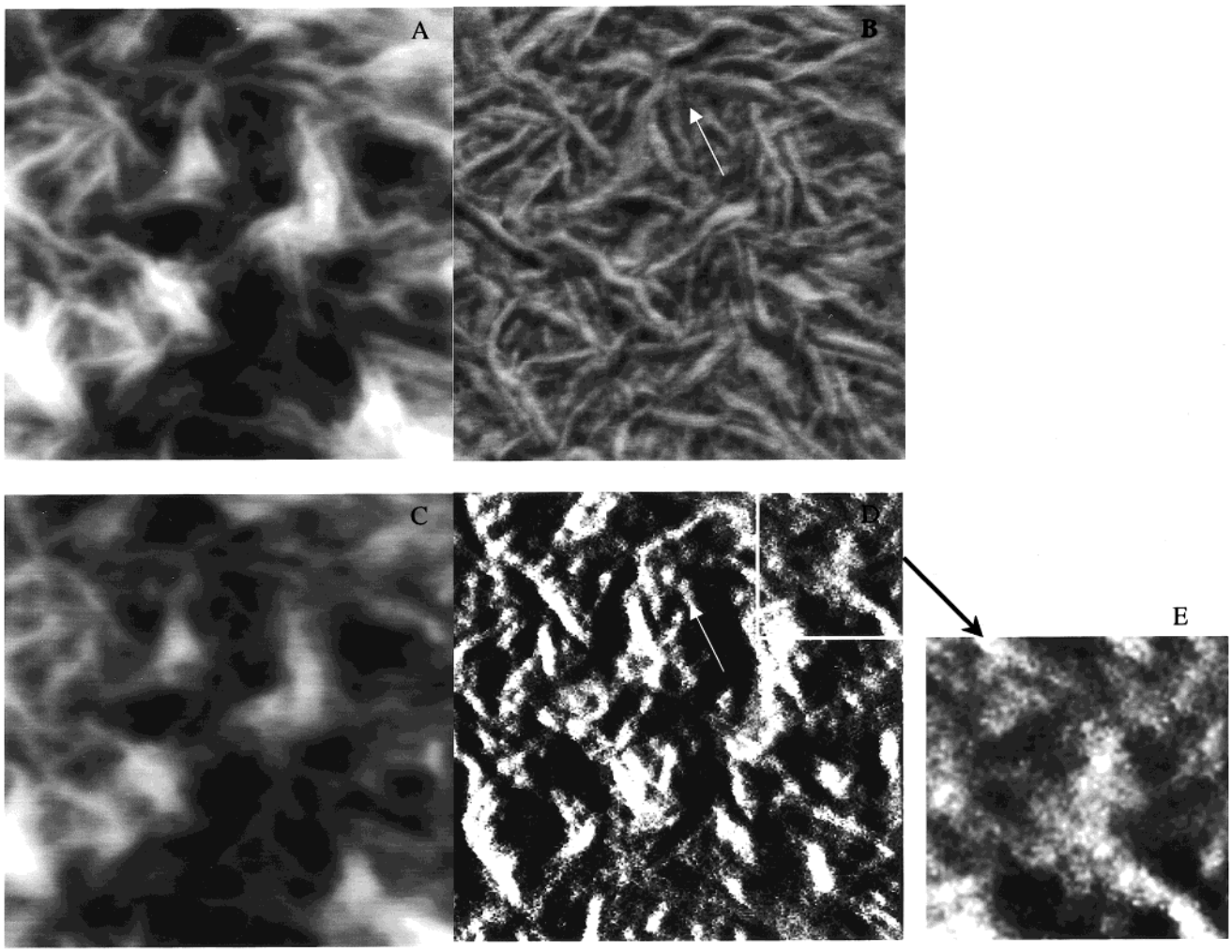

Figure 2. Images of a Surlyn Zn18 surface in AFM normal (A, B) and low oscillation amplitude (C−E) tapping. The surface was prepared by cooling from 190 to 25 °C, annealing at 90 °C for 2 min, before cooling back to room temperature. The height data from normal (A) and low oscillation energy (C) tapping show some similarities, while the phase data in (B) and (D) on the same spots show dramatic differences. Normal tapping phase data (B) are sensitive to stiffness contrast, and low oscillation amplitude tapping (D) derives its contrast from ionic-rich regions just below the surface (see text). Arrows indicate representative soft (dark) regions in the normal tapping phase data (B), and the exact corresponding spots are indicated in (D), indicating high populations of ionic species (light) in low oscillation amplitude tapping. The identical 500 × 500 nm spot was studied in (A)−(D), and (E) is a magnified (150 nm × 150 nm) region from the boxed area in (D). The scales are 0−10 nm for height data and 0−20° for phase data.

this layer, and one must consider that this may lower the contrast and sharpness of boundaries of lamellae imaged below the surface.

Phase images sequentially taken under normal (Figure 2B) followed by low oscillation amplitude (D) conditions are distinctly different, while the height data from normal (A) and low oscillation energy (C) tapping are similar although contrast is somewhat better in (A). The identical 500 × 500 nm spot was studied in this comparison. Normal tapping phase data are sensitive to stiffness differences and exhibit mainly the details of lamellar organization in Figure 2B, somewhat similar to the normal tapping height data in Figure 2A. In Figure 2D the contrast is derived from ionic concentration differences near the surface. If ionic domains have the same "stiffness" as amorphous polyethylene, then we should not expect any contrast from ionic domains with AFM in normal "phase" imaging as is found in Figure 2B. To help guide the eye, we have provided arrows that point to the soft regions where lamellae are absent (darker regions in Figure 2A−C), with the identical points marked in Figure 2D. The comparison shows that these correspond to bright regions rich in ionic domains. Many ionic domains are clustered into these white regions and cannot be individually resolved in Figure 2D because they are overlapped with each other. Many separate ones are resolvable as small white dots in Figure 2D and have diameters on the order of 2 nm consistent with recent SAXS data and analysis which gave a diameter of 1.7 nm for a slightly different Surlyn material[42] and with high-resolution TEM which gave diameters of about 2−3 nm depending on thermal history.[21,22] Figure 2E gives a magnified view of the indicated region from Figure 2D, and ionic domain sizes on the order of 2−3 nm in diameter are relatively well resolved in several regions. The contribution of interphase species and possibly reduced resolution due to the ionic domains residing at some finite and even variable depth beneath the hydrocarbon layer make the AFM somewhat qualitative. We have taken higher magnification scans, but the resolution of single ionic domains is not improved significantly, possibly because of larger degrees of sample deformation because of the higher residence time of the tip on the surface during the

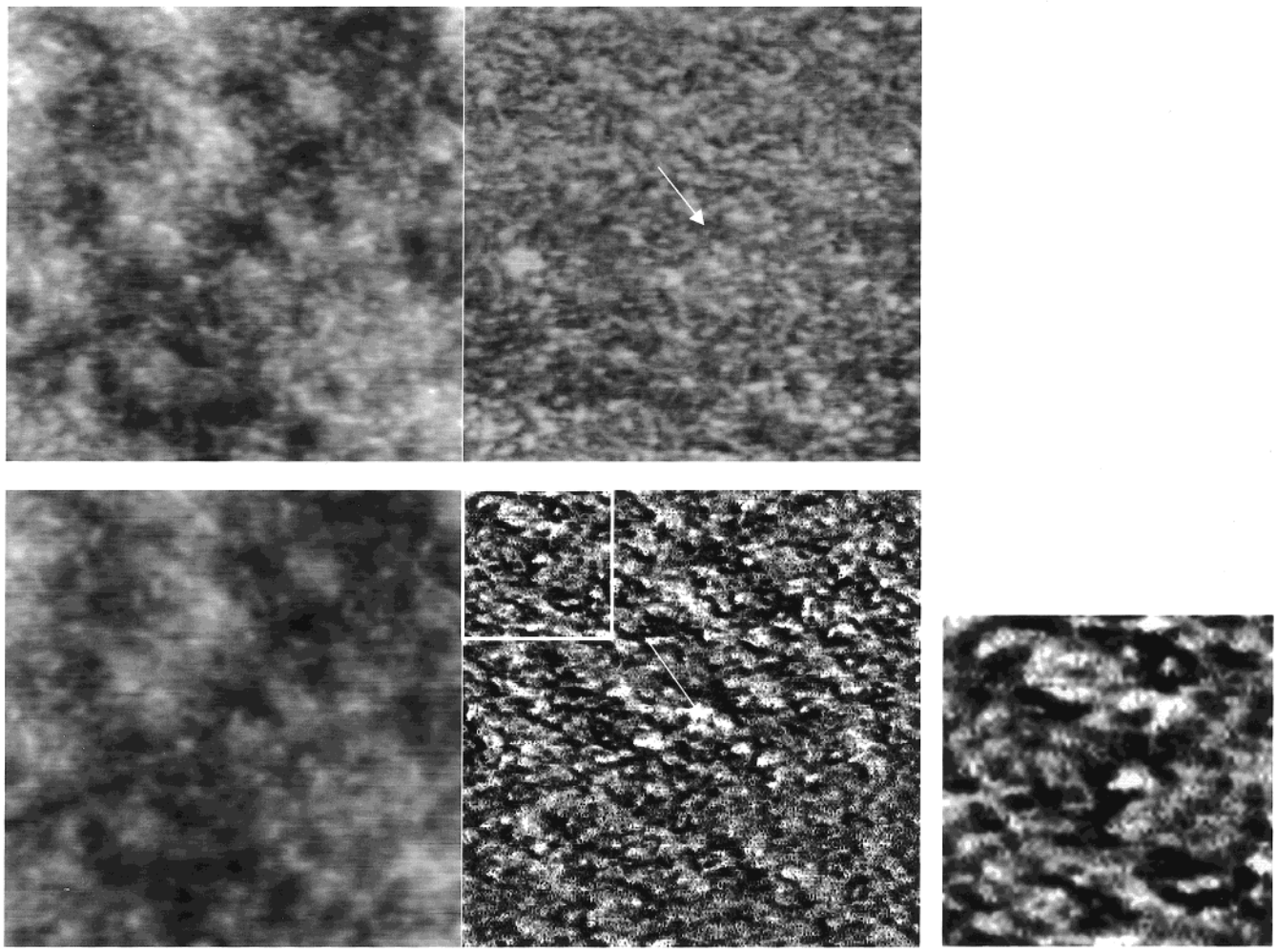

Figure 3. Images of a Surlyn Na54 surface in AFM normal (A, B) and low oscillation amplitude (C−E) tapping. The surface was prepared by cooling from 190 to 25 °C, annealing at 90 °C for 2 min, before cooling back to room temperature. The height data from normal (A) and low oscillation energy (C) tapping show some similarities, while the phase data in (B) and (D) on the same spots show dramatic differences. Arrows indicate representative soft (dark) regions in the normal tapping phase data (B), and the exact corresponding spots are indicated in (D), indicating high populations of ionic species (light) in low oscillation amplitude tapping. The identical 500 × 500 nm spot was studied in (A)−(D), and (E) is a magnified (150 nm × 150 nm) region from the boxed area in (D). The scales are 0−10 nm for height data and 0−20° for phase data.

lateral scanning at a constant scan frequency. This lack of improved resolution in very high magnification AFM scans was also discussed in previous studies of nanoseparated copolymer systems.[28]

Parts B and D of Figure 2 were not taken simultaneously but were carefully obtained rescans over the same imaged region. The importance of this is that any contributions of thermal drift and other factors which could contribute to an offset would make much of the interpretation invalid. Parts A and B of Figure 2 were first obtained simultaneously, then height and phase data were obtained by scanning from the bottom of the imaged region (not shown), and finally parts C and D of Figure 2 were obtained by scanning from the top again. The offset could be gauged from the various nanofeatures and was about 3 nm for the first two experiments and less than a nanometer between Figure 2A,B compared to Figure 2C,D. Thus, we can prove that thermal drift can be minimal even for very high magnification scans.

Figure 3 shows tapping data for Surlyn Na54 which has a somewhat different lamellar morphology because of the higher degree of acid comonomer and especially higher level of neutralization (Table 1) compared to Surlyn Zn18 in Figure 2. Simultaneously obtained AFM height and phase data for Surlyn Na54 were obtained under normal tapping conditions (Figure 3A,B) and show the dramatically smaller lamellae present because of the higher level of acid and neutralization. Each scan box in Figure 3A−D is 500 nm × 500 nm. The ionic domains are not sensed or imaged in Figure 3A,B because the data were obtained under normal tapping conditions. The ethylene lamellae show organization into parallel orientations to differing degrees and barely show any anisotropy in dimensions. Phase images sequentially taken under normal (Figure 3B) followed by low oscillation amplitude (D) conditions show distinctly different contrast and different length-scale morphologies. The height data from normal (A) and low oscillation energy (C) tapping are similar, as was the case in the series of experiments in Figure 2. Normal tapping phase data are sensitive to stiffness differences and exhibit mainly the details of lamellar organization in Figure 3B, somewhat similar to the normal tapping height data in Figure 3A. In Figure 3D the contrast is derived from ionic domains near the surface. To help guide the eye, we have provided arrows that point to the soft regions where lamellae are absent (darker

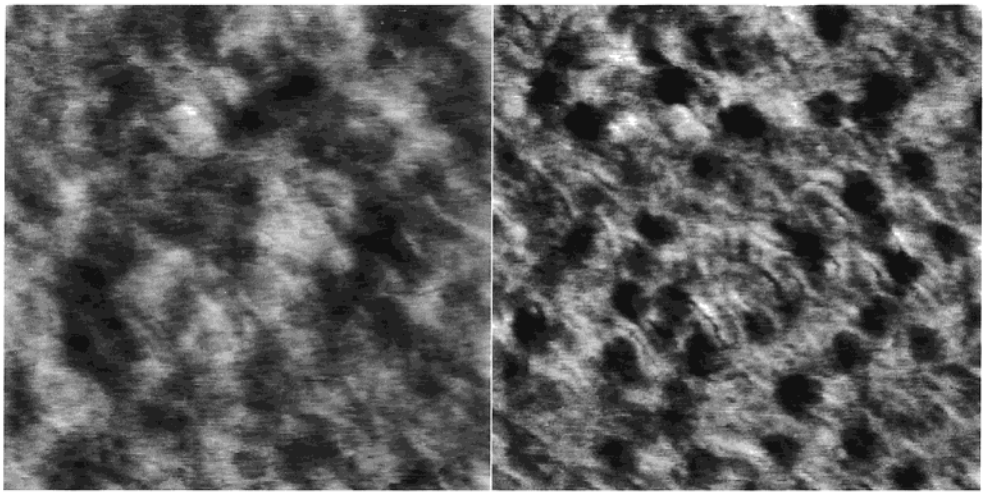

Figure 4. AFM normal tapping height (A) and "phase" (B) data for a Surlyn Na54 film surface. The surface was prepared by cooling from 190 to 25 °C at 20 °C/min with the surface in contact with silicon. The height data on the left show short- and long-range roughness, and the phase data on the right give similar but better resolved details of lamellar morphology. Scan boxes are 300 × 300 nm for each plot, and the height and phase scales are 0−5 nm and 0−20°, respectively.

regions in Figure 3A−C) and have compared these to the identical points in Figure 3D that correspond to bright regions rich in ionic domains, verifying that the ionic domains concentrate away from regions rich in lamellae. Many ionic domains are clustered into the most ionic rich (whiter) regions and sometimes cannot be individually resolved. Many separate ones are resolvable as small white dots in Figure 3D and have diameters on the order of 2 nm, consistent with recent SAXS data and analysis which gave a diameter of 1.7 nm for a slightly different Surlyn material and with high-resolution TEM which gave diameters of about 2−3 nm with very monodisperse sizes. Figure 3E gives a magnified view of the indicated region from Figure 3D, and ionic domain sizes on the order of 2−3 nm in diameter are relatively well resolved in several regions.

The following images were taken using normal tapping in order to examine some effects of counterion and acid content on the lamellar structure only. All of the following sample surfaces were prepared by cooling from the melt at ca. 190 °C at 20 °C/min with no other annealing. Data taken on a different Surlyn Na54 surfaces in Figure 4 show again that the crystals are imperfect and sparse due to high levels of acid and neutralization. Small crystal thicknesses of 5 nm are extracted, and values of L from AFM are approximately consistent with SAXS (Table 1). There is much discussion in the literature on the appropriate analysis procedure for SAXS data for systems with imperfect lamellae and negligible or small degrees of lamellar stacking.[25] AFM helps to define the details of the structures, including the lateral dimensions which are not available from SAXS at all. Figure 5 (top) shows two more images of Zn18 in different regions on the surface. The crystals fill the space quite uniformly and have some structures resembling row-nucleated morphologies where several lamellae grow perpendicular to a central "primary" lamellae.[43] They cannot be row-nucleated structures in the usually described sense[43] because presumably in Figure 5 (top) the chain orientation in the central lamellae is perpendicular to the chain direction in the subsidiary lamellae because both contain the usual chain folded crystals in these nonoriented systems. Relatively uniform space filling of imperfect lamellae are seen on a different region of the surface (Figure 5, bottom). The acid and neutralization levels are low in Surlyn Zn18, contributing to the perfected and more densely packed crystals in Surlyn Zn18 relative to Na54. Figure 6 shows the imperfect crystals in Surlyn Zn58, although they fill the space better than a Na neutralized sample (Na54) of about the same acid content, e.g., compare with Surlyn Na54 in Figures 3 and 4.

Nucrel is the acid form and because of the absence of counterions exhibits relatively large crystals (Figure 7) with some doublet structures seen in several of the images. This is also a general future in many metal neutralized samples such as Surlyn Zn18 in Figures 2 and 5. Doublets are seen to be the dominant structures in many regions relative to single lamellae or triplets. This could be related to the nature of segregation and exclusion of ionic species from the growing lamellae, depleting the crystallizable species from the region outside of the growing lamellae and restricting the development of thick stacks of lamellae. The crystals seem to be the longest laterally in Nucrel probably because of the known higher mobility in the melt. Low oscillation energy tapping AFM phase results detected no contrast in terms of resolving ionic domains or even clumps of ionic rich regions presumably because of the well-known lack of ionic domain structures in systems such as Nucrel.[23] It is known that, without metal neutralization, ionic domain formation is restricted or prohibited.

Surlyn Na59 has an even higher acid content than Na54, and since they are both Na neutralized and Na neutralization gives ionomers with the highest melt viscosities, it is not surprising that the crystals are very imperfect in Na59 (Figure 8). Many crystals are detected near the surface, but they are barely anisotropic and the lateral perfection is the poorest of all the samples. The resolution of many of the crystals is also poor. The low degree of lateral perfection leads to a relatively low SAXS peak intensity for the lower angle peak related to the lamellar spacing (Figure 1, see the region of $2\theta = \sim 1.2°$); thus, these two methods of characterization are qualitatively consistent.

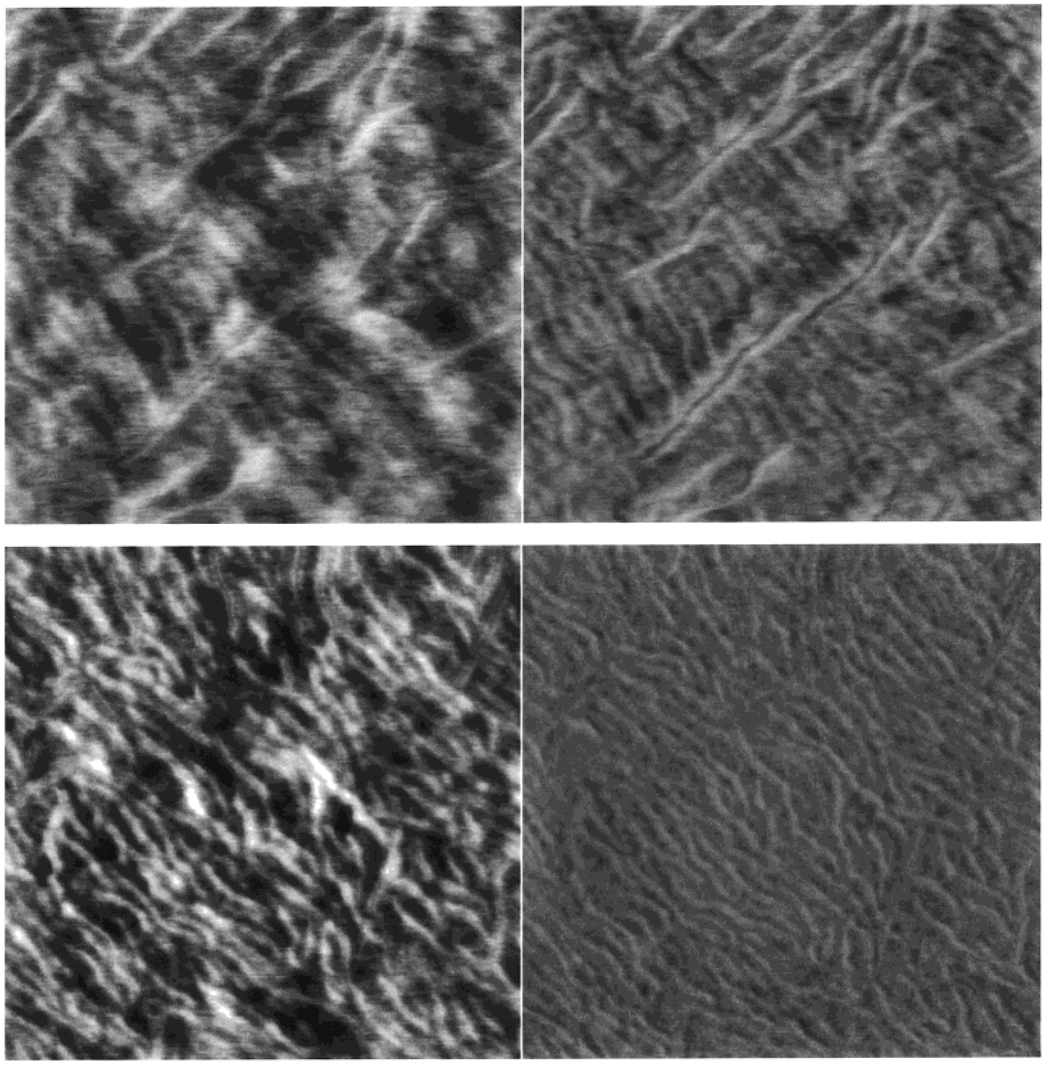

Figure 5. AFM normal tapping height (A, C) and "phase" (B, D) data for different regions of a Surlyn Zn18 film surface. The surface was prepared by cooling from 190 to 25 °C at 20 °C/min. Scan boxes are 300 × 300 nm for each plot, and the height and phase scales are 0−5 nm and 0−20°, respectively.

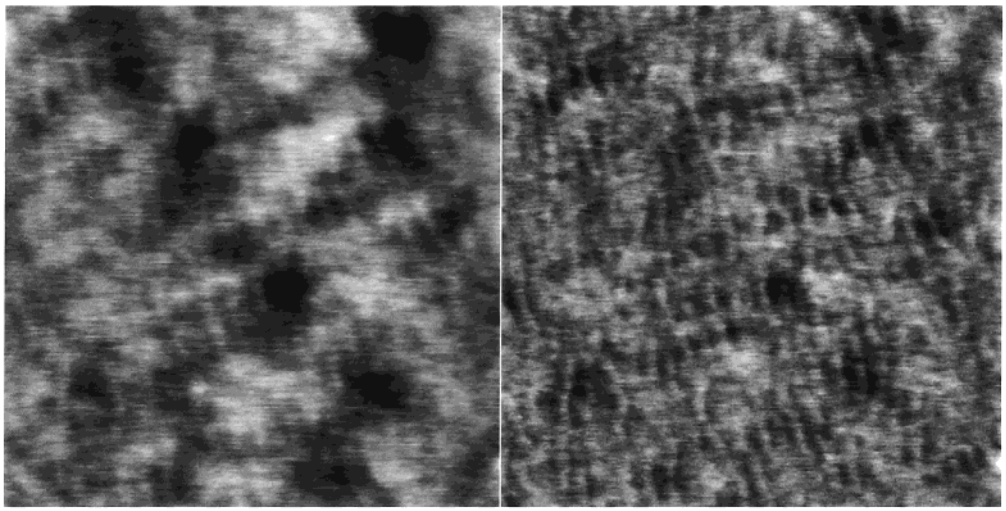

Figure 6. AFM normal tapping height (A) and "phase" (B) data for a Surlyn Zn58 film surface. The surface was prepared by cooling from 190 to 25 °C at 20 °C/min. Scan boxes are 300 × 300 nm for each plot, and the height and phase scales are 0−5 nm and 0−20°, respectively.

Contrasting the AFM characterization of the degree of crystallinity with that determined by wide-angle X-ray diffraction (WAXD) and thermal (DSC) analysis shows some interesting differences. DSC gives a moder-

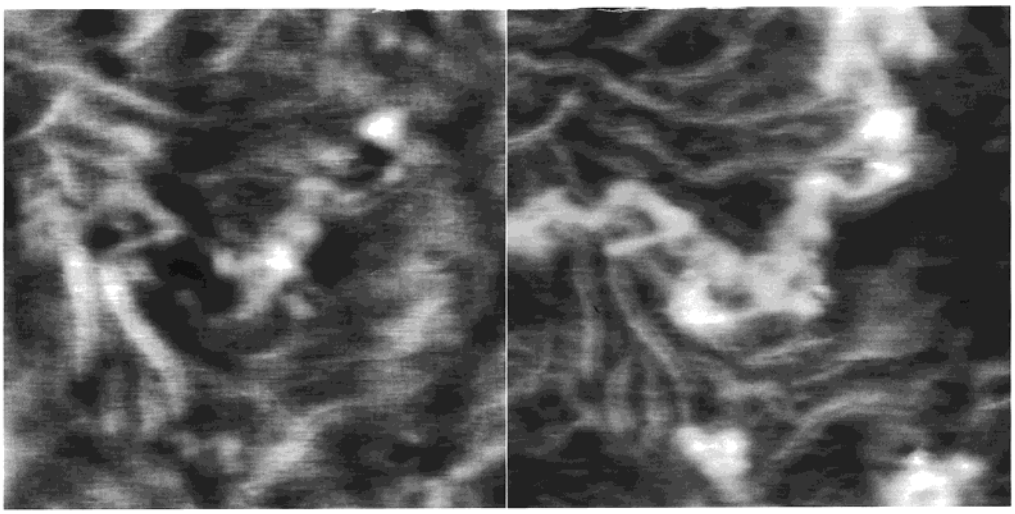

Figure 7. AFM normal tapping height (A) and "phase" (B) data for a Nucrel (unneutralized acid form of the ethylene copolymers) film surface. The surface was prepared by cooling from 190 to 25 °C at 20 °C/min. Many curved lamellae are detected, and most are in the form of doublets. Scan boxes are 300 × 300 nm for each plot, and the height and phase scales are 0−5 nm and 0−20°, respectively.

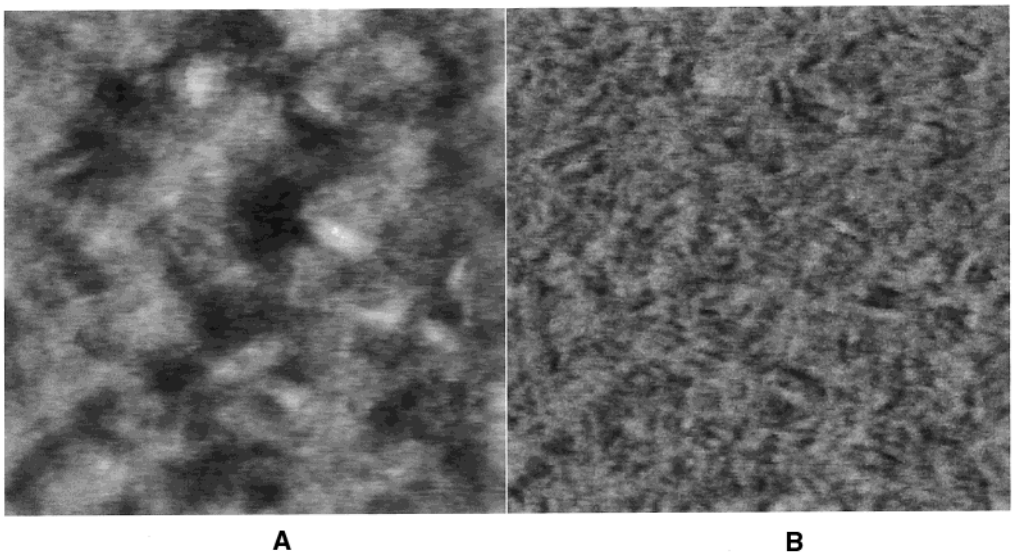

Figure 8. AFM normal tapping height (A) and "phase" (B) data for a Surlyn Na59 film surface. The surface was prepared by cooling from 190 to 25 °C at 20 °C/min. Scan boxes are 300 × 300 nm for each plot, and the height and phase scales are 0−10 nm and 0−15°, respectively.

ate degree of crystallinity (heat of fusion was measured to be 50 J/g for Na59 which converts to ~18% crystallinity), and the SAXS peak due to the lamellar diffraction is reasonably distinct (Figure 1), but WAXD barely detects any crystallinity and gives a percent crystallinity (crystallinity index) below 5%. The simple explanation is that the lateral perfection of the lamellae is insufficient for diffraction reducing the WAXD crystalline intensity, and this is a relatively general feature of copolymers and other systems with imperfect crystals.[25] DSC data for Surlyn Zn18 give a heat of fusion of 95 J/g corresponding to 33% crystallinity. This is consistent with the relatively high level of crystal perfection detected by AFM and SAXS.

One of the last samples that we melt pressed with the silane-treated silicon wafer was another Surlyn (Figure 9) with a composition similar to Na59 but with slightly lower neutralization levels. The data shown were also obtained at a lower magnification than in the images discussed above. This silicon wafer was previously used for about 15 melt surface preparations. One can see black dots in the height data on the left, and these are found to be small flat holes about 1.2 ± 0.2 nm deep. These dots are very small, and we found them on all polymer surfaces pressed at about that time. Upon imaging the silane-treated wafer, we found that the silane "monolayer" was no longer a monolayer but had very small patches with only a few percent surface coverage which exactly replicated the inverse of the Surlyn surface (Figure 9). This is one interesting method of making features a few nanometers in dimension on a material's surface.

Finally, as with all imaging techniques it is difficult to present enough information to characterize the entire system. Another surface preparation of an unannealed Surlyn Zn18 sample gave some hint of lamellae which were face-on, as opposed to the more common situation where the sample surface consists of mostly of edge-on orientations (Figure 10). In most regions doublet structures characterize the lamellae which have a relatively

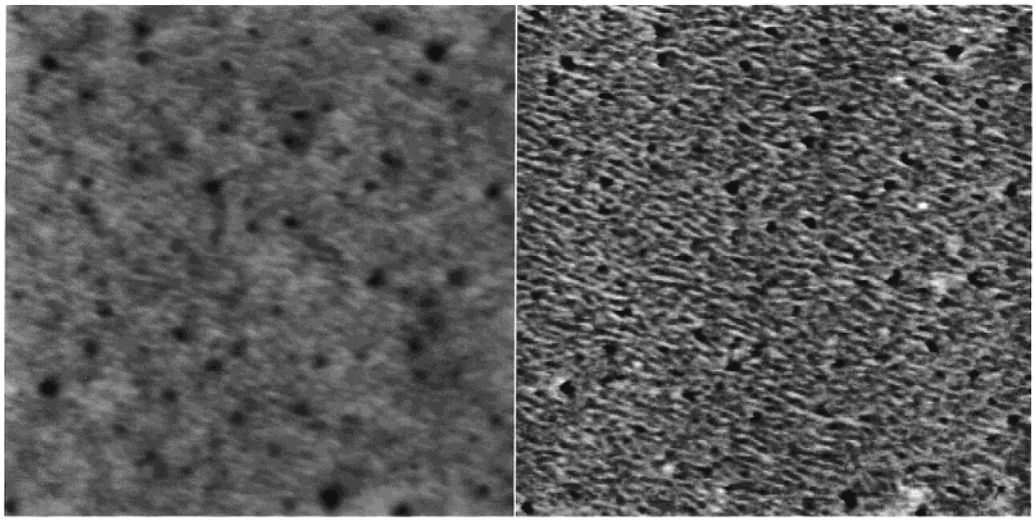

Figure 9. Lower magnification AFM normal tapping height (A) and "phase" (B) data for a film surface of a polymer with slightly lower neutralization levels than Surlyn Na59. The surface was prepared by cooling from 190 to 25 °C at 20 °C/min with the surface in contact with a silanated silicon wafer surface. See text for a description of the factors in sample preparation which cause the small holes in the height data. Scan boxes are 1000 × 1000 nm for each plot, and the height and phase scales are 0−20 nm and 0−20°, respectively.

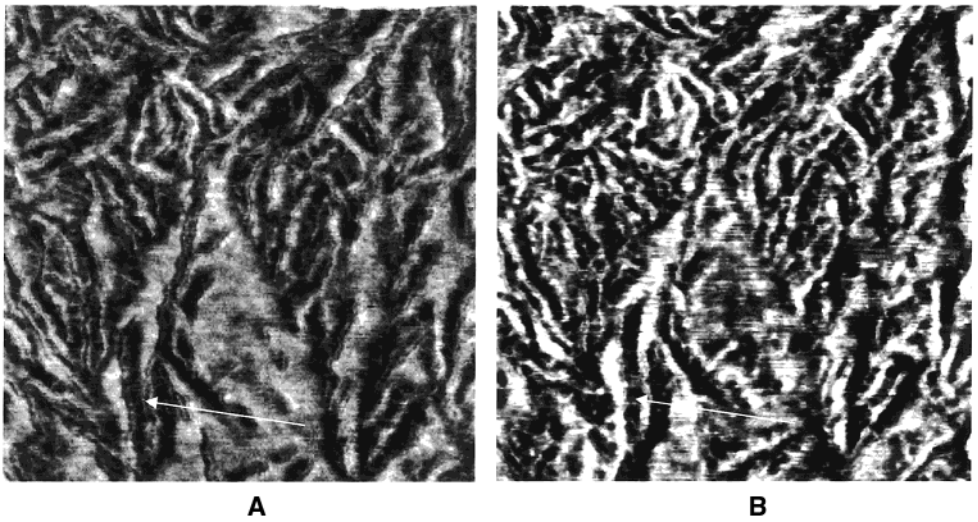

Figure 10. AFM phase data for an unannealed Surlyn Zn18 surface taken using of normal (A) and low oscillation amplitude (B) tapping. No height data are shown. Scan boxes are 500 × 500 nm for each plot, and the phase scales are 0−20° for both images. Arrows indicate a representative hard (light) region in the normal tapping phase data (A), and the exact corresponding spot is indicated in (B), indicating depleted populations of ionic species (dark) in low oscillation amplitude tapping (see text).

high aspect ratio, and although not obvious from cursory visual inspection, from computer analysis comparing identical spots in Figure 10A,B there is excellent correlation between dark regions depleted of crystals on the left and bright ionic rich regions on the right, and vice versa. The broad regions in the middle of the scan box with a moderate hardness (Figure 10A) may be face-on lamellae and correspond to regions with relatively low ionic concentrations (Figure 10B). Remember that normal tapping can detect hard domains down to depths about 10 nm beneath the surface, so the species covering lamellae of all orientations can be complicated, but in general ionic-rich regions are scarce on top of the face-on lamellae in Figure 10.

Discussion

AFM phase data give the ethylene lamellar dimensions and spacings listed in Table 1. Approximate dispersities in the thicknesses and spacings from these real space data are represented by the range of values in the table, and the thicknesses are somewhat qualitative because of the unknown contributions of tip radii, tilting of lamellae under the surface, and various interface contributions. The lamellae are anisotropic in length to differing degrees with lengths typically between 50 and 100 nm (Table 1). Small-angle X-ray scattering characterization of both the ionic interdomain distances (L_{IP}) and the lamellar crystal spacings (L) of the hydrocarbon segments in metal neutralized Surlyn polymer samples has been extensively reported.[2,13,23,42] The values of L from AFM (Table 1) are approximately consistent with those from SAXS data (Figure 1), which gave 10, 9, and 8 nm for Zn18, Na54, and Na59, respectively. The amorphous interlayer thickness between parallel lamellae is qualitatively characterized and is about 4 nm from AFM, and broader noncrystalline gaps outside of the ordered lamellar regions are typically around 10 nm or greater in dimension (Figure

2B, for example). These broader "gaps" of softer material were also shown to be rich in ionic species and domains. This latter information is somewhat unique to real-space characterization techniques.

Starting with the other coarser length-scale aspects of ionic domain morphology which are mainly characterized by low oscillation energy AFM, the ionic domains are found to be clumped together in the form of anisotropic ~10−15 nm wide and several tens of nanometers long ionic-rich regions consisting of multiple (partially overlapped) ionic domains in the AFM images in Figure 2D or 3D. The clumping is in part from the exclusion from lamellar phases and/or restrictions in formation of ionic domains where they may be partially or mostly excluded from entire stacks of oriented lamellae. The stacks are admittedly imperfect here, so this cannot be generalized for all semicrystalline ionomers at this time. The widths of the more concentrated clumps of ionic domains resolved by low oscillation energy AFM (Figure 2D) are broader than the individual lamellae thicknesses obtained by normal tapping AFM (e.g., Figure 2B where lc is found to be ~5 nm). We must be aware that AFM detects morphologies near the surface, but not exactly at the surface (see Experimental Section). This could complicate the apparent position of ionic species relative to lamellae, especially if normal tapping (stiffness contrast) can detect lamellae underneath amorphous and/or ionic-rich thin overlayers because of the deeper probe depth of the normal tapping measurement believed to be on the order of at least 5−10 nm below the surface. Furthermore, the morphology and composition of the surface region relative to the bulk are always a concern.

Turning to finer length-scale morphologies, AFM images in Figures 2 and 3 suggest that there is some level of exclusion of ionic domains from crystal lamellae as is expected because the crystals could not exist if they contained ionic domains. These data also suggest that ionic domains are at least partially excluded from the thin layers between stacked lamellae, even though the lamellar stacks are admittedly imperfect in the Surlyn samples studied here, especially in Figure 3. The explanation could be related to the limited "amorphous" space and lowered number of mobile species within the lamellar stacks. Register and Cooper[23] have proved by SAXS, where electron densities of the various phases were estimated, that there are some ionic species and/or domains between stacked lamellae. Quiram, Register, and Ryan[13] also showed some evidence for exclusion of ionic domains from lamellar stacks after crystallization where a larger shift in the SAXS ionomer peak occurred compared to that expected for a relatively low level of crystallinity development. This is consistent with some of the AFM evidence for clumped regions rich in ionic domains separate from ethylene lamellae. The SAXS experiment is less sensitive to the nonperiodic regions outside of the stacked lamellae, so AFM provides information on some of the morphological features not detectable by SAXS. SAXS gives 1.7 nm diameter domains and values of L (average spacing from center to center) equal to 2.8 nm, showing that domains are closer together in the clumped regions than expected on the basis of the bulk volume fraction of ionic species.[42] Gierke et al. [7] have also characterized the close to space-filling nature of ionic domains in the ionic-rich regions in a few "dry" perfluorinated sulfonic acid (Nafion) membrane systems. STEM techniques applied to Surlyn[21,22] demonstrate higher resolution for individual ionic domains relative to low oscillation energy AFM. STEM gives ionic domain diameters of 2−3 nm depending on thermal history and neutralization level. The domains were shown to be spherical with a reasonably low level of dispersity in sizes.[21,22]

Finally, we consider the two most fundamental yet controversial issues of ionic domain morphology, the factors which govern the size of the domains and the spacing between domains. The previously proposed model developed mostly to explain the SAXS data considers the effect of the "layer of bound hydrocarbon on the surface of the aggregate" which necessarily provides a limit of the nearest approach distance of two ionic domains.[2] This model was shown to apply to a variety of ionomers including noncrystalline ones.

We now turn to a discussion of steric effects due to chain structure which we believe are dominant in limiting the domain size. Steric effects arise from the "random" nature of the polymer chain and the constraints which evolve due to the chain stretching as ionic species attempt to migrate into domains. If the ionic and nonionic regions (domains) become too large at the typical low volume fraction of ionic species, then these backbone chains cannot stretch enough to allow incorporation of species into ionic domains because increases in ionic domain sizes must occur simultaneously with increases in hydrocarbon "domain" dimensions. The low volume fraction of ionic groups effectively keeps the domain morphology in a regime of dispersed spheres because of steric chain constraints, as opposed to cylindrical or lamellar morphologies which are common in phase separating copolymers only at higher volume fractions of the minor block.

In addition, an important factor that is almost never considered in modeling of these systems is the effect of interfacial tension which is a strong driving force for increasing the domain size and must be considered in addition to the well-known enthalpy of interaction of ion pairs and multiplets.[3,5,12] Interfacial tension would also drive these systems toward spheres which are the minimum surface area state. The steric effects due to the above chain architecture effects oppose these enthalpic driving forces, and the result is the well-defined domain sizes (Figure 2e) which are not highly polydisperse and do not even vary in size substantially with neutralization level.[22] These chain architecture effects also limit the domain size to a few nanometers in a variety of nonionic "segmented" polymers[28] which are definitely not random because of the synthetic procedure giving chains which consist of well-defined hard and soft block lengths and include segmented polyurethanes and others. Critical factors in defining the domain sizes and shapes include the block sizes and total volume fraction of the segregating minor phase. This contribution of steric chain effects must be considered separately from the crystal-induced conformational restrictions which also possibly limit increases in ionic domain size, keeping in mind that the SAXS data which show the presence of strong ionic domain scattering in the Surlyn crystal-free melt,[13] suggesting that the crystal induced constraints are less important.

Conclusions

AFM methods were applied to resolve the surface and near-surface morphology of the ionic domains in Surlyn ionomers. Tapping AFM using normal "stiffness" con-

trast was used to resolve the ethylene-rich lamellae near the surface, and additional AFM techniques were developed to resolve the ionic-rich regions, characterizing individual circular ionic domains on the order of 2−3 nm in dimension in selected regions. The different degrees of parallel organization of ethylene lamellae and row-nucleated morphologies in some Surlyn compositions were characterized, with ionic domains and clumps of ionic domains partially segregated into broader regions sometimes outside of the defective "lamellar stacks" in these low-crystallinity systems containing imperfect crystal organization. Stacks are defined as the regions of approximately parallel lamellae. AFM has the advantage that the dimensions and anisotropy of the lamellae or crystallites are determined in real space, in addition to characterizing the dispersity in sizes and the relative positions and orientations in space.

The ionic domains in these materials were resolved by a new AFM method utilizing low oscillation amplitudes where tip/ionic-cluster attractive interactions dominate the signal, facilitating nanometer-level resolution of the domains. Annealing the samples led to an improvement in the resolution of individual ionic domains. Sequential images taken under different AFM conditions showed that the "softer" regions depleted of lamellae contained ionic domains in the same topographical areas. In addition, the overall morphology of the dispersion of ionic domains and ionic-rich regions was characterized. Because of the somewhat limited resolution and the way AFM detects the domains at slightly varying depths below the surface, many of the ionic domains appear overlapped.

SAXS characterization of both individual ionic domain separation and ethylene lamellar spacings is established in the literature.[2,13,23,42] SAXS data obtained for Surlyn samples with different levels of neutralization were used to confirm the AFM analysis and to contrast details of the resolution of both techniques.

Acknowledgment. We thank Dr. B. Wood for suggesting many of the experiments and for critical comments on the manuscript. We also thank Mr. D. Brill, Mr. R. Davidson, and Dr. D. Londono for their contributions to the characterization by X-ray techniques.

References and Notes

(1) Longworth, R.; Vaughan, D. J. *Polym. Prepr. (Am. Chem. Soc., Div. Polym. Chem.)* **1968**, *9*, 525.
(2) Yarusso, D. J.; Cooper, S. L. *Polymer* **1985**, *26*, 371.
(3) Mauritz, K. A. *J. Macromol. Sci., Rev. Macromol. Chem. Phys.* **1988**, *C28* (1), 65.
(4) Tant, M. R.; Wilkes, G. L. *J. Macromol. Sci., Rev. Macromol. Chem. Phys.* **1988**, *C28* (1), 1.
(5) Eisenberg, A.; Hird, B.; Moore, R. B. *Macromolecules* **1990**, *23*, 4098.
(6) Eisenberg, A.; Kim, J.-S. *Introduction to Ionomers*; John Wiley & Sons: New York, 1998.
(7) Gierke, T. D.; Munn, G. E.; Wilson, F. C. *J. Polym. Sci., Polym. Phys.* **1981**, *19*, 1687.
(8) Gierke, T. D.; Hsu, W. Y. In *Perfluorinated Ionomer Membranes*; Eisenberg, A., Yeager, H. L., Eds.; ACS Symposium Series No. 180; American Chemical Society: Washington, DC, 1982; Chapter 13, p 283.
(9) Yeager, H. L.; Steck, A. *J. Electrochem. Soc.* **1981**, *128*, 1880.
(10) Fujimura, M.; Hashimoto, T.; Kawai, H. *Macromolecules* **1981**, *14*, 1309.
(11) Fujimura, M.; Hashimoto, T.; Kawai, H. *Macromolecules* **1983**, *15*, 136.
(12) Eisenberg, A. *Macromolecules* **1970**, *3*, 147.
(13) Quiram, D. J.; Register, R. A.; Ryan, A. J. *Macromolecules* **1998**, *31*, 1432.
(14) Yarusso, D. J.; Cooper, S. L. *Macromolecules* **1983**, *16*, 1871.
(15) Roche, E. J.; Stein, R. S.; MacKnight, W. J. , *J. Polym. Sci., Polym. Phys. Ed.* **1980**, *18*, 1035.
(16) Marx, C. L.; Caulfield, D. F.; Cooper, S. L. *Macromolecules* **1973**, *6*, 344.
(17) Roche, E. J.; Stein, R. S.; Russell, T. P.; MacKnight, W. J. *J. Polym. Sci., Polym. Phys. Ed.* **1980**, *18*, 1497.
(18) MacKnight, W. J.; Taggart, W. P.; Stein, R. S. *J. Polym. Sci., Polym. Symp.* **1974**, *45*, 113.
(19) Grady, B. P. *Macromolecules* **1999**, *32*, 2983.
(20) Welty, A.; Ooi, S.; Grady, B. P. *Macromolecules* **1999**, *32*, 2989.
(21) Laurer, J. H.; Winey, K. I. *Macromolecules* **1998**, *31*, 9106.
(22) Winey, K. I.; Laurer, J. H.; Kirkmeyer, B. P. *Macromolecules* **2000**, *33*, 507.
(23) Register, R. A.; Cooper, S. L. *Macromolecules* **1990**, *23*, 318.
(24) Biswas, A.; Brill, D. J. Personal communication.
(25) Vanden Eynde, S.; Mathot, V.; Koch, M. H. J.; Reynaers, H. *Polymer* **2000**, *41*, 3437.
(26) Magonov, S. N.; Whangbo, M.-H. *Surface Analysis with STM and AFM*; VCH: Weinheim, 1996.
(27) Magonov, S. N.; Elings, V.; Whangbo, M.-H. *Surf. Sci. Lett.* **1997**, *375*, L385.
(28) McLean, R. S.; Sauer, B. B. *Macromolecules* **1997**, *30*, 8314.
(29) Hild, S.; Gutmannsbauer, W.; Lüthi, R.; Fuhrmann, J.; Güntherodt, H.-J. *J. Polym. Sci., Polym. Phys.* **1996**, *34*, 1953.
(30) Kravchenko, R. L.; Sauer, B. B.; McLean, R. S.; Keating, M. Y.; Cotts, P. M.; Kim, Y. H. *Macromolecules* **2000,** 33, 11.
(31) Magonov, S.; Godovsky, Y. *Am. Lab.* **1999**, April, 52.
(32) McLean, R. S.; Sauer, B. B. *J. Polym. Sci., Polym. Phys.* **1999**, *37*, 859.
(33) Chomakoba-Haefke, M.; Nyffenegger, R.; Schmidt, E. *Appl. Phys. A* **1994**, *59*, 151.
(34) Lehmani, A.; Durand-Vidal, S.; Turq, P. *J. Appl. Polym. Sci.* **1998**, *68*, 503.41. Brandsch, R.; Bar, G.; Whangbo, M.-H. *Langmuir* **1997**, *13*, 6349.
(35) James, P. J.; McMaster, T. J.; Newton, J. M.; Miles, M. J. *Polymer* **2000**, *41*, 4223.
(36) McLean, R. S.; Doyle, M.; Sauer, B. B. *Macromolecules* **2000**, *33*, 6541.
(37) Sagiv, J. *J. Am. Chem. Soc.* **1980**, *102*, 92.
(38) Brandsch, R.; Bar, G.; Whangbo, M.-H. *Langmuir* **1997**, *13*, 6349.
(39) Sauer, B. B.; McLean, R. S.; Thomas, R. R. *Langmuir* **1998**, *14*, 3045.
(40) Matyi, R. J.; Crist, B. *J. Polym. Sci., Polym. Phys.* **1973**, *11*, 635.
(41) Crist, B.; Morosoff, N. *J. Polym. Sci., Polym. Phys.* **1973**, *11*, 1023.
(42) Verma, R.; Hsiao, B. S.; Biswas, A. *Am. Chem. Soc. Prepr., Polym. Div.* **1998**, *39* (1), 54.
(43) Bassett, D. C. *Principles of Polymer Morphology*; Cambridge University Press: New York, 1981; p 189.

MA001110T